

无节点反谐振空芯光纤 1064 nm 高功率皮秒脉冲传输

鲁文举^{1,2,3}, 张鑫^{1,2,3}, 朱宽^{1,2,3}, 杜可明⁴, 王璞^{1,2,3*}¹北京工业大学材料与制造学部,北京市激光应用技术工程技术研究中心,北京 100124;²北京工业大学跨尺度激光成型制造技术教育部重点实验室,北京 100124;³北京工业大学激光工程研究院,北京 100124;⁴Edgewave 公司, Würselen 52146, 德国

摘要 本文报道了利用自制低损耗、无节点反谐振空芯光纤传输高功率 1064 nm 皮秒脉冲激光的研究。光纤包层由 7 根平均壁厚为 700 nm 的细玻璃管组成,纤芯直径为 42 μm ,外径为 175 μm 。选择脉冲宽度为 15 ps 且重复频率可调谐的高功率激光器作为实验光源。使用不同长度的光纤进行了传输测试,测试结果表明:当输入单脉冲能量为 403 μJ 、平均功率为 40.3 W、峰值功率为 26.8 MW 的激光时,最高可实现 370 μJ 的高能量激光输出,传输效率高达 91.8%。分析了超短脉冲经过不同长度光纤后时域和频域的变化情况,结果表明:当光纤长度为 1 m 时,脉冲保持无畸变传输,光谱发生轻微变形;当光纤长度增长至 3.3 m 时,由于非线性效应的影响,脉冲宽度展宽至 26 ps,光谱展宽至 70 nm。本研究表明无节点反谐振空芯光纤有望在超短脉冲激光的传输应用领域发挥重要作用。

关键词 激光光学;超短脉冲传输;无节点反谐振空芯光纤;峰值功率;单脉冲能量;非线性效应

中图分类号 TN253

文献标志码 A

doi: 10.3788/CJL202249.0306001

1 引言

激光柔性传输能够避免复杂光路的限制,传输激光更灵活、便捷,在机械加工、激光医疗、国防技术等领域^[1-3]有着广阔的应用前景。近年来,随着激光技术的迅猛发展,激光器向着更短脉冲、更高能量、更高功率的方向快速迈进,因此对光纤柔性激光传输的需求也越来越高。传统的实芯光纤存在低材料损伤阈值、高色散和高非线性等本征材料缺陷,这些缺陷使得石英光纤在传输超短脉冲激光时只能承受纳焦耳量级的能量^[4],并且很难避免光纤损伤或脉冲畸变的产生^[5]。对于光波而言,最完美的传输介质是无非线性、无色散、无损耗的真空环境。空芯光子晶体光纤(HC-PCF)通过玻璃微结构将光束束缚在空气纤芯中传播,提供了近乎自由空间的传播条件。历经 20 多年的发展,HC-PCF 的光学性能得到了极大提升^[6-14],在高功率超短脉冲传输方面展现出了巨大潜力。

早期利用 HC-PCF 传输超短脉冲激光的工作大多围绕空芯光子带隙光纤(HC-PBGF)展开。2010 年,巴斯大学的 Knight 研究团队^[15]使用 1 m 长 7 芯 HC-PBGF 实现了平均功率为 500 mW、脉冲宽度为 100 fs 的激光输出。2016 年,南安普顿大学的 Richardson 研究团队^[16]使用 37 芯 HC-PBGF 在 1 μm 实现了平均功率为 2.2 W、脉冲宽度为 90 fs 的超短脉冲传输,对应的峰值功率为 300 kW,单脉冲能量为 27 nJ。HC-PBGF 的导光原理决定了它存在传输带宽较窄的弊端,并且纤芯基模与玻璃结构重叠面积较大,导致损伤阈值不高^[17],因此,利用 HC-PBGF 传输的激光单脉冲能量仅为百纳焦耳量级,峰值功率普遍不高。与 HC-PBGF 相比,空芯反谐振光纤(HC-ARF)具有更大的模场面积、更宽的导光通带和更高的损伤阈值,因此有着更高的超短脉冲传输潜力。2014 年,苏黎世联邦理工学院的研究人员^[18]对 66 cm 长 Kagome 型反谐振光纤纤芯进行氩气填充,实现

收稿日期: 2021-04-06; 修回日期: 2021-05-11; 录用日期: 2021-06-08

基金项目: 国家重点研发计划(2017YFB0405200)、国家自然科学基金重点项目(62035002)

通信作者: *wangpuemail@bjut.edu.cn

了平均功率为 118 W、单脉冲能量为 18 μJ 、脉冲宽度为 22 ps 的超短脉冲输出,输出的峰值功率大于 20 MW;但是,充气使实验装置变得复杂,不便于实际应用。2016 年,NKT 公司^[19]使用 5 m 长 HC-ARF 实现了中心波长为 1032 nm、脉冲宽度为 22 ps 的超短脉冲传输,输出的平均功率超过 70 W,但是传输的单脉冲能量仅为 7 μJ ,峰值功率仅为 318 kW。2017 年,本课题组^[20]使用自制的 HC-ARF 实现了中心波长 1032 nm 处单脉冲能量为 185 μJ 、峰值功率为 10.8 MW 的超短脉冲传输,但是光纤长度只有 1 m,并且耦合效率不高,仅为 68%。因此,在考虑激光传输过程对光纤传输损耗、弯曲性能以及损伤阈值等综合需求的基础上,实现高功率、高能量超短脉冲激光的高效率传输具有重要意义。

本课题组使用实验室自制的低损耗无节点反谐振空芯光纤进行了超短脉冲激光柔性传输的研究。首先利用中心波长为 1064 nm、脉冲宽度为 15 ps、重复频率可调谐的皮秒激光光源实现了单脉冲能量为 403 μJ 、平均功率为 40.3 W、峰值功率为 26.8 MW 的超短脉冲传输,接着分析了超短脉冲经过不同长度光纤后时域和频域的变化特性,最后验证了无节点反谐振空芯光纤在超短脉冲传输应用方面的超高潜力。

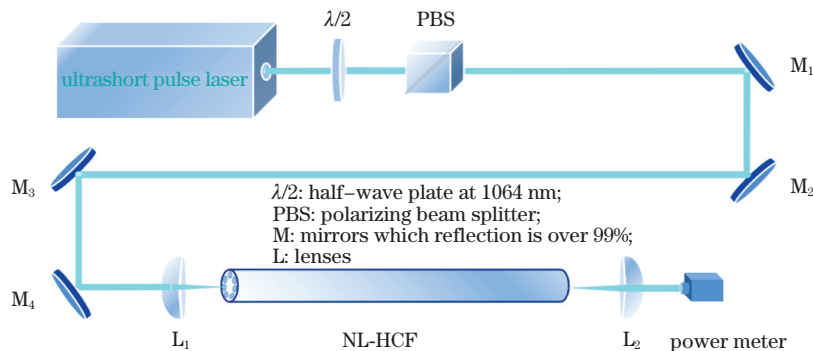


图 1 无节点反谐振空芯光纤空间传输实验装置

Fig.1 Experimental device for space propagation of nodeless anti-resonant hollow-core fibre (NL-HCF)

2.2 无节点反谐振空芯光纤

本课题组使用一款实验室自制的无节点反谐振空芯光纤进行实验。光纤端面的扫描电子显微镜图如图 1(a)所示,可见:光纤包层中有 7 个直径为 24 μm 的毛细玻璃管,包层石英壁厚均匀,约为 700 nm,包层玻璃管围成的纤芯直径(内切圆直径)为 42 μm ,光纤外径为 175 μm 。利用超连续光源(光谱覆盖 450 ~ 2400 nm)将光耦合进长度为 200 m 的光纤中,使用 AQ6370C 型光谱仪采集光

2 实验装置及无节点反谐振空芯光纤介绍

2.1 实验装置

本文使用的激光光源为德国 Edgewave 公司生产的一台中心波长为 1064 nm、脉冲宽度为 15 ps、重复频率可调谐的皮秒激光器。在重复频率设定为 100 kHz 的情况下,激光器输出激光的最大单脉冲能量可达 470 μJ ,平均功率为 47 W,峰值功率为 31.3 MW。使用固定焦距的透镜将光束聚焦,利用光束轮廓分析仪(BeamScope-P8)探测、采集聚焦光束的束腰以及束腰两侧的多组光斑数据,然后进行拟合处理,计算得激光器的光束质量因子为 1.25 ± 0.05 。

搭建如图 1 所示的高功率超短皮秒脉冲传输测试装置。激光器输出的光束通过半波片($\lambda/2$)和偏振光分束器(PBS)进行功率调制,在调节功率的同时保证传输系统输入光束的稳定性。使用 4 个高反射率反射镜($M_1 \sim M_4$)准直光束并调整激光入射的角度。将待测光纤固定于 V 型槽并放置在高精度三维调整架上,平凸透镜(L_1)将光束聚焦到光纤的输入端。选择合适的焦距实现入射激光与光纤的模式匹配,通过精准调节三维调整架将聚焦后的激光耦合进光纤中,最后对输出光束进行功率测量及光学性能表征。

谱信息,测得光纤输出端功率为 P_1 ;然后,保持耦合端状态不变,将光纤截短至 5 m,再次测得光纤输出端功率为 P_2 。将 P_1 和 P_2 代入(1)式计算光纤的损耗谱。

$$\alpha(\lambda) = \frac{10 \lg(P_2/P_1)}{L}, \quad (1)$$

式中: L 是截断光纤的长度,单位为 km。光纤的传输谱及损耗谱如图 2(b)所示,其中,曲线①为光纤传输 200 m 后的光谱,曲线②为截短至 5 m 的光纤

的传输光谱。可以看出,该光纤二阶传输带宽为 780~1200 nm(谱线 1060 nm 附近的尖峰是超连续

谱自带的残余抽运光)。曲线③是计算得出的损耗谱,在 1064 nm 附近的光纤损耗为 50 dB/km。

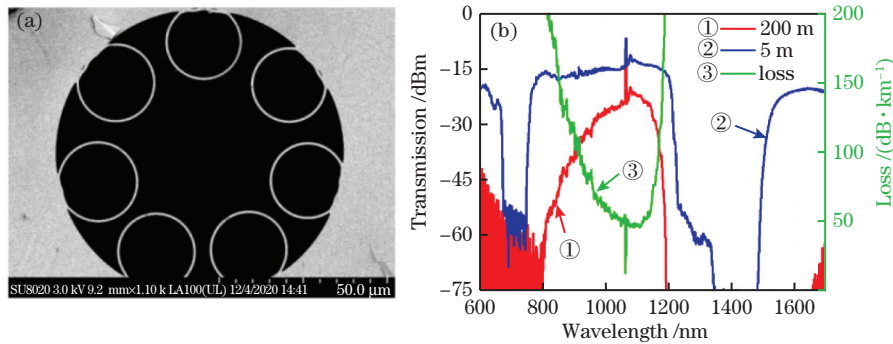


图 2 无节点反谐振空芯光纤的电子显微镜图以及传输谱和损耗谱。(a)电子显微镜图;(b)传输谱和损耗谱

Fig. 2 SEM image, transmission and loss spectra of fabricated NL-HCF. (a) SEM image; (b) transmission and loss spectra

考虑到光纤在应用过程中弯曲是不可避免的,因此测量了这款光纤在不同弯曲直径下于 1064 nm 波长处的弯曲损耗,以探究其传输皮秒脉冲的衰减情况。首先将激光耦合进 3 m 长光纤中,测得光纤在平直情况下的输出功率 P_2 ,并将该输出功率作为基准;保持耦合端状态不变,分别将光纤弯曲直径调整为 20 cm(3 圈)、30 cm(2 圈)、40 cm(2 圈)和 50 cm(1 圈),此时测得输出端的功率为 P_1 。采用(1)式计算弯曲损耗,此时的 L 为光纤弯曲的实际长度。弯曲损耗的计算结果如表 1 所示,可以看出,随着弯曲直径增大,弯曲损耗显著降低,弯曲直径为 50 cm 时,弯曲损耗仅为 0.015 dB/m。

表 1 无节点反谐振空芯光纤在 1064 nm 波长处的弯曲损耗

Table 1 Bending loss of NL-HCF at 1064 nm	
Bending diameter/cm	Bending loss / (dB·m ⁻¹)
20	0.37
30	0.1
40	0.03
50	0.015

3 高功率超短脉冲激光传输实验

皮秒脉冲激光器输出的准直光束的直径为 2.3 mm,实验选取的是焦距为 50 mm 的平凸透镜,其聚焦后的光斑直径(1/e²)为 30 μm(光纤模场直径约为 31.5 μm),匹配度较高,有利于实验的进一步开展。

在实验中,本课题组选择了 1 m 和 3.3 m 两种不同长度的光纤进行传输测试,其中 1 m 长光纤保持平直状态;考虑到弯曲损耗和光纤使用的常用环境,将 3.3 m 长光纤以 30 cm 的弯曲直径盘绕两

圈。首先剥掉光纤端面 5 cm 厚的涂覆层并将其固定于 V 型槽中,将百毫瓦的低功率激光准直后聚焦于光纤端面,以避免对二氧化硅包层造成损坏。通过实时监测光纤输出端功率的变化情况来精确调节三维调整架 X、Y、Z 轴的位置,逐步将耦合状态调至最佳;此时保持耦合状态不再改变,逐渐提升输入激光的脉冲能量,测试不同脉冲功率下光纤输出端功率的变化情况。由图 3 可以看出:随着激光输入功率的增加,光纤输出端的功率呈线性增大的趋势;当激光器输入最大单脉冲能量为 403 μJ、平均功率为 40.3 W、峰值功率为 26.8 MW 的皮秒脉冲时,长度 1 m 的光纤能够以 91.8% 传输效率输出单脉冲能量为 370 μJ、平均功率为 37 W 的皮秒脉冲激光;当光纤长度增加至 3.3 m 时,仍将耦合状态调至最佳,由于光纤长度的增加和引入的弯曲损耗的共同影响,输出激光的最大单脉冲能量降至 347 μJ,平均功率为 34.7 W,传输效率变为 86%。从多次实

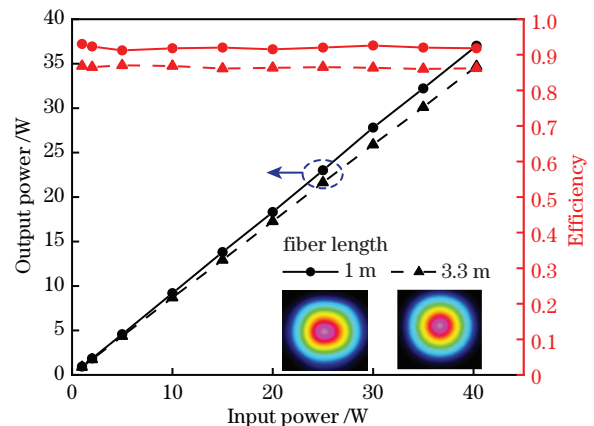


图 3 超短脉冲激光经过不同长度无节点反谐振空芯光纤的传输效率

Fig. 3 Propagation efficiency of ultra-short pulse laser passes through different lengths of NL-HCF

验情况来看,在上述输入的皮秒脉冲参数下,这款光纤端面未见损伤,而且在保证耦合端状态不改变的前提下,轻轻触碰或移动光纤,仍能够保持稳定传输。此外,在光纤输出端测得了接近衍射极限的光束,图 3 中的内嵌图为光纤末端输出的近场模式分布图。光纤输出的激光比入射激光有着更低的光束质量因子,其中:光纤长度为 1 m 时,计算得到的光束质量因子为 1.14 ± 0.05 ;光纤长度为 3.3 m 时,计算得到的光束质量因子为 1.07 ± 0.05 。光纤长度的增加以及弯曲的引入使得高阶模被快速损耗掉,因此输出光束质量得以优化。

本课题组使用 $1 \mu\text{m}$ 自相关仪对脉冲激光的时域特性进行了表征。图 4 给出了超短脉冲激光经过无节点反谐振空芯光纤前后的自相关迹变化,其中:黑色虚线是输入激光的脉冲宽度 15 ps;实线①是经过 1 m 长 NL-HCF 后输出超短脉冲的自相关迹,可以看出输出的脉冲与激光器初始脉冲的形状、宽度一致,没有任何变化,此时光纤输出激光的峰值功率达到了 24.6 MW;实线②是经过 3.3 m 长 NL-HCF 后输出超短脉冲的自相关迹,可以看出此时输出激光的脉冲宽度已经展宽至 26 ps,对应的输出峰值功率降到 13.2 MW。

本课题组进一步研究了激光脉冲的频域特性。首先测量了输入激光的脉冲,并将其作为参考。实验中采集了不同输入单脉冲能量下的光谱数据,如图 5 所示。由图 5(a)可以看出:当输入单脉冲能量低于 $215 \mu\text{J}$ 时,经过 1 m 无节点反谐振空芯光纤的激光脉冲的光谱形状与入射激光的光谱形状相同,

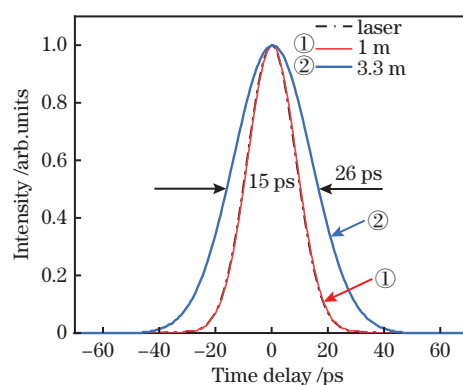


图 4 超短脉冲激光经过不同长度无节点反谐振空芯光纤的自相关迹

Fig. 4 Autocorrelation traces of ultra-short pulse laser passes through different lengths of NL-HCF

光谱轻微展宽;当单脉冲能量高于 $215 \mu\text{J}$ 后,光谱逐渐受到自相位调制(SPM)效应的影响,光谱形状开始发生轻微形变,但并不严重。在保持耦合条件不变的前提下,3.3 m 长光纤中的非线性效应显著增强,光谱中出现了更复杂的结构,如图 5(b)所示。当输入单脉冲能量低于 $100 \mu\text{J}$ 时,光谱能保持原有的形状;当输入单脉冲能量在 $100 \sim 234 \mu\text{J}$ 范围内时,自相位调制效应逐渐增强;当输入单脉冲能量大于 $234 \mu\text{J}$ 后,部分光子被纤芯中的空气分子散射,分子转移到更高频率的振动状态,在受激拉曼散射(SRS)效应的影响下,一阶斯托克斯拉曼峰和反斯托克斯拉曼峰分别出现在 1070 nm 和 1057 nm ;随着输入激光单脉冲能量的继续提升,输出光谱中出现了更高阶的斯托克斯光和反斯托克斯光,当输入单脉冲能量增加到 $403 \mu\text{J}$ 时,光谱已展宽至近 70 nm 。

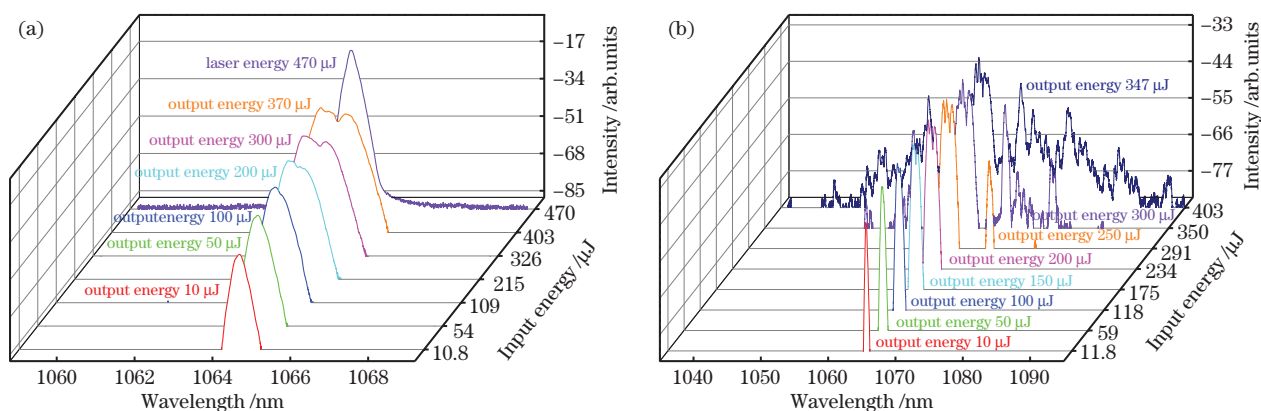


图 5 不同输入单脉冲能量下输出光谱的变化。(a) 1 m 长无节点反谐振空芯光纤;(b) 3.3 m 长无节点反谐振空芯光纤
Fig. 5 Variations of output spectra at different input single-pulse energies. (a) 1 m NL-HCF; (b) 3.3 m NL-HCF

4 结 论

本课题组基于光纤高功率传输过程对传输损耗、弯曲性能以及激光损伤阈值的综合需求,报道了

实验室控制的低损耗近红外导光的无节点反谐振空芯光纤在高功率皮秒脉冲传输领域的应用。所用光纤的包层由 7 根平均壁厚为 700 nm 的细玻璃管组成,纤芯直径为 $42 \mu\text{m}$,外径为 $175 \mu\text{m}$,其在

1064 nm 附近的传输损耗为 50 dB/km, 弯曲损耗为 0.1 dB/m(30 cm 直径)。本课题组使用这款光纤实现了中心波长为 1064 nm、脉冲宽度为 15 ps、单脉冲能量为 403 μ J、平均功率为 40.3 W、峰值功率为 26.8 MW 的皮秒脉冲传输, 获得了接近衍射极限的光束输出, 且光纤端面未见损伤。此外, 本课题组对比了 1 m 和 3.3 m 两种长度光纤的传输特性, 结果发现: 长度为 1 m 的光纤能够以 91.8% 传输效率输出平均功率为 37 W 的激光, 对应输出的单脉冲能量为 370 μ J, 脉冲宽度未发生变化, 光谱轻微展宽, 峰值功率达到 24.6 MW; 光纤长度增至 3.3 m 时, 在相同的输入条件下, 光纤以 86% 的传输效率和 34.7 W 的平均功率保持激光的稳定输出, 单脉冲能量为 347 μ J; 输出的激光比入射激光有着更低的光束质量因子, 且光纤长度的增加以及弯曲的引入能够提升光束质量。但是, 光纤长度增加的同时会增强非线性效应, 从而对传输激光脉冲的时域和频域产生一定程度的影响, 因此在实际应用过程中, 需要对光纤长度的选择进行权衡, 或者可以通过纤芯抽真空、充特定气体等方式来减轻非线性效应的影响。

参 考 文 献

- [1] Audouard E, Lopez J, Ancelot B, et al. Optimization of surface engraving quality with ultrafast lasers[J]. *Journal of Laser Applications*, 2017, 29(2): 022210.
- [2] Zhou Y Y, Xiao Y C, Sun L J, et al. Optical-fiber fluorescent probes [J]. *Laser & Optoelectronics Progress*, 2020, 57(1): 010003.
周艳焰, 肖永川, 孙力军, 等. 光纤荧光探针[J]. *激光与光电子学进展*, 2020, 57(1): 010003.
- [3] Lian Z G, Chen X, Wang X, et al. Preparation and potential applications of microstructured and integrated functional optical fibers [J]. *Laser & Optoelectronics Progress*, 2019, 56(17): 170615.
廉正刚, 陈翔, 王鑫, 等. 微结构和集成式功能光纤的制备和潜在应用[J]. *激光与光电子学进展*, 2019, 56(17): 170615.
- [4] Smith A V, Do B T. Bulk and surface laser damage of silica by picosecond and nanosecond pulses at 1064 nm[J]. *Applied Optics*, 2008, 47(26): 4812-4832.
- [5] Skuja L, Hosono H, Hirano M. Laser-induced color centers in silica [J]. *Proceedings of SPIE*, 2001, 4347: 155-168.
- [6] Mangan B J, Farr L, Langford A, et al. Low loss (1.7 dB/km) hollow core photonic bandgap fiber[C] // *Optical Fiber Communication Conference*, February 23-27, 2004, Los Angeles, CA, USA. New York: IEEE Press, 2004, 2: 3.
- [7] Wang Y Y, Wheeler N V, Couny F, et al. Low loss broadband transmission in hypocycloid-core Kagome hollow-core photonic crystal fiber [J]. *Optics Letters*, 2011, 36(5): 669-671.
- [8] Debord B, Alharbi M, Benoît A, et al. Ultra low-loss hypocycloid-core Kagome hollow-core photonic crystal fiber for the green spectral-range applications [C] // *2014 Conference on Lasers and Electro-Optics (CLEO)-Laser Science to Photonic Applications*, June 8-13, 2014, San Jose, CA, USA. New York: IEEE Press, 2014: 1-2.
- [9] Yu F, Knight J C. Spectral attenuation limits of silica hollow core negative curvature fiber [J]. *Optics Express*, 2013, 21(18): 21466-21471.
- [10] Gao S F, Wang Y Y, Liu X L, et al. Bending loss characterization in nodeless hollow-core anti-resonant fiber [J]. *Optics Express*, 2016, 24(13): 14801-14811.
- [11] Gao S F, Wang Y Y, Ding W, et al. Hollow-core conjoined-tube negative-curvature fibre with ultralow loss[J]. *Nature Communications*, 2018, 9(1): 2828.
- [12] Jason G T, Bradley T D, Harrington K, et al. Hollow core NANF with 0.28 dB/km attenuation in the C and L bands [C] // *2020 Optical Fiber Communications Conference and Exhibition (OFC)*, March 8-12, 2020, San Diego, CA, USA. New York: IEEE Press, 2020: 1-3.
- [13] Gao S F, Wang Y Y, Wang P. Research progress on hollow-core anti-resonant fiber and gas Raman laser technology[J]. *Chinese Journal of Lasers*, 2019, 46(5): 0508014.
高寿飞, 汪滢莹, 王璞. 反谐振空芯光纤及气体拉曼激光技术的研究进展[J]. *中国激光*, 2019, 46(5): 0508014.
- [14] Xia C M, Zhou G Y. Progress and prospect of microstructured optical fibers [J]. *Laser & Optoelectronics Progress*, 2019, 56(17): 170603.
夏长明, 周桂耀. 微结构光纤的研究进展及展望[J]. *激光与光电子学进展*, 2019, 56(17): 170603.
- [15] Mosley P J, Huang W C, Welch M G, et al. Ultrashort pulse compression and delivery in a hollow-core photonic crystal fiber at 540 nm wavelength[J]. *Optics Letters*, 2010, 35(21): 3589-3591.
- [16] Chen Y, Mulvad H C H, Sandoghchi S R, et al. First demonstration of low loss, bend insensitive 37-cell hollow-core photonic bandgap fiber at 1 μ m for high power delivery applications[C] // *2016 Conference on Lasers and Electro-Optics (CLEO)*, June 5-10,

- 2016, San Jose, CA, USA. New York: IEEE Press, 2016: 1-2.
- [17] Michaille L F, Taylor D M, Bennett C R H, et al. Damage threshold and bending properties of photonic crystal and photonic band-gap optical fibers [J]. Proceedings of SPIE, 2004, 5618: 30-38.
- [18] Emaury F, Saraceno C J, Debord B, et al. Efficient spectral broadening in the 100-W average power regime using gas-filled kagome HC-PCF and pulse compression [J]. Optics Letters, 2014, 39 (24): 6843-6846.
- [19] Michieletto M, Lyngsø J K, Jakobsen C, et al. Hollow-core fibers for high power pulse delivery [J]. Optics Express, 2016, 24(7): 7103-7119.
- [20] Gao S F, Wang Y Y, Liu X L, et al. Hollow-core anti-resonant fiber and its use for propagation of high power ultrashort pulse [J]. Chinese Journal of Lasers, 2017, 44(2): 0201012.
- 高寿飞, 汪滢莹, 刘小璐, 等. 空芯反谐振光纤及其高功率超短脉冲传输 [J]. 中国激光, 2017, 44(2): 0201012.

Propagation of High-Power Picosecond Pulse at 1064 nm Using Nodeless Anti-Resonant Hollow-Core Fibre

Lu Wenju^{1,2,3}, Zhang Xin^{1,2,3}, Zhu Kuan^{1,2,3}, Du Keming⁴, Wang Pu^{1,2,3*}

¹Beijing Engineering Research Center of Laser Technology, Faculty of Materials and Manufacturing, Beijing University of Technology, Beijing 100124, China;

²Key Laboratory of Trans-Scale Laser Manufacturing Technology (Beijing University of Technology), Ministry of Education, Beijing 100124, China;

³Institute of Laser Engineering, Beijing University of Technology, Beijing 100124, China;

⁴Edgewave GmbH, Würselen 52146, Germany

Abstract

Objective Ultra-short pulse laser provides unprecedented experimental means and extreme physical conditions for the study of light-matter interactions owing to its extremely short pulse duration and ultra-high peak power. It is used in waveguide etching, attosecond science, biomedicine, industrial processing, and many other fields. Presently, most high-power ultra-short pulse laser propagation systems currently use multiple reflectors and other optical devices to control and propagate lasers. Too many devices not only increase the complexity of the system but also reduce the transmission efficiency of the laser, which limits its application range. This is primarily owing to basic material defects in traditional solid-core fibres, such as high nonlinearity, low damage threshold, and high dispersion, which means solid-core fibres can only support nanojoule energy when propagating ultra-short pulse laser, and avoiding fibre damage or pulse distortion is difficult. Anti-resonant hollow-core fibre (AR-HCF) is designed with a specific cladding microstructure that confines the optical field in the air core, avoiding the absorption and damage as solid-core fibres, as well as providing a nearly ideal environment with low nonlinearity, time delay, dispersion, and loss. This enables it to propagate high-power ultra-short pulsed lasers in the range of a few metres flexibly and stably.

Methods This study is based on a homemade nodeless anti-resonant hollow-core fibre(NL-HCF). First, to ensure the stability of the input laser when adjusting the power, the laser's output beam is controlled using a half-wave plate and polarisation beam splitter. Four high reflectivity mirrors are used to collimate the laser and adjust the angle of incidence. Then the NL-HCF is fixed in the V-groove and placed on the 3-axis stage. A plane-convex lens focuses the laser on the NL-HCF's input. A suitable focal length is chosen to achieve mode field matching between the laser and the fibre. The focused laser is coupled into the fibre by precisely adjusting the 3-axis stage. Finally, the output power of the fibre is measured, and the time-domain and frequency-domain properties of the laser passing through the NL-HCF are characterised.

Results and Discussions The NL-HCF we used has a 42 μm fibre core, 175 μm outer diameter, and six capillaries in the cladding with a 700 nm thick wall. At 1064 nm, the confinement loss is 50 dB/km, and the bending loss is 0.1 dB/m@30 cm diameter. We used two lengths of 1 and 3.3 m NL-HCF for propagation tests, in which the fibre length of 1 m was kept straight and the fibre length of 3.3 m was coiled twice with a bending diameter of 30 cm. The

output power of NL-HCF increased linearly as the input laser power increased. When coupling a pulse with a single pulse energy of $403 \mu\text{J}$, an average power of 40.3 W , and a pulse width of 15 ps , we got a 91.8% propagation efficiency with the maximum output pulse energy of $370 \mu\text{J}$ and average power of 37 W by 1 m NL-HCF (Fig. 3). The output pulse was consistent with the original pulse's shape and width, corresponding to a peak power of 24.6 MW of the output laser, and the spectrum was slightly deformed. Then, we increased the fibre length to 3.3 m . Under the same conditions, the maximum single pulse energy of the output laser decreased to $347 \mu\text{J}$, the average power decreased to 34.7 W , the propagation efficiency became 86% . The output laser's pulse width was increased to 26 ps (Fig. 4), and the peak output power was reduced to 13.2 MW . The self-phase modulation and stimulated Raman scattering effects broadened the spectrum to 70 nm (Fig. 5).

Conclusions In this study, we explored the high-power pico-second pulse propagation characteristics using a homemade low-loss NL-HCF. During the high-power propagation of NL-HCF, the fibre was chosen to meet the comprehensive requirements of confinement loss, bending performance, and laser damage threshold. The pulse width of the light source was 15 ps , and its repetition frequency was adjustable. Different lengths of NL-HCF were used for propagation tests. When the input laser was coupled to the NL-HCF with a $403 \mu\text{J}$ pulse energy, 40.3 W average power, and 26.8 MW peak power, we obtained a 91.8% propagation efficiency with a maximum output pulse energy of $370 \mu\text{J}$. We analysed the spectral and temporal characteristics of ultra-short pulse passing through different NL-HCF lengths. When the NL-HCF length was 1 m , the laser pulse was propagated without distortion, and the spectrum was slightly deformed. Owing to the non-linear effect, the pulse width of the output laser was increased to 26 ps and the spectrum was expanded to 70 nm when the length of the NL-HCF was increased to 3.3 m . Experiments show that NL-HCF will play an important role in the propagation of ultra-short pulses.

Key words laser optics; ultra-short pulse propagation; nodeless anti-resonant hollow-core fibre; peak power; single pulse energy; non-linear effect